Stochastic cracking of brittle matrix composites with heterogeneous reinforcement

Rostislav Rypl and Rostislav Chudoba
Institute of Structural Concrete, RWTH Aachen University, Germany

Miroslav Vořechovský
Institute of Structural Mechanics, Brno University of Technology, Czech Republic

Abstract. A model capable of capturing the effect of irregularly structured reinforcement in a brittle matrix is presented. It introduces a homogenization procedure for the state fields at the microscale in the vicinity of a crack bridge. In combination with a mesoscale model for matrix cracking the homogenized state fields are used for explicit calculation of the strain hardening-response of the composite. The model has been formulated for brittle matrix composites with reinforcement that exhibits random properties, e.g. due to random fiber orientation or because of an irregular penetration profile of the matrix into multifilament yarns. In the present paper we use multifilament yarns applied in textile reinforced concrete (TRC) to demonstrate the capabilities of the model. It is used for parametric studies to detect some qualitative and quantitative dependencies between the micromechanical material parameters and strain-hardening response of the composite.

Keywords: stochastic cracking, multifilament yarn, statistics, composite strength, micromechanics, filament

1. Introduction

Combining brittle matrix with fibrous reinforcement leads to quasi-ductile composite behavior with a high bearing capacity. When loaded in tension brittle matrix composites exhibit multiple cracks developing in the matrix perpendicularly to the loading direction (Li and Wu, 1992; Fantilli *et al.*, 2009). This process is accompanied with significant stress redistributions both between and within the constituents of the composite. The qualitative and quantitative characteristics of composites depend on the mechanical and geometrical properties of the components and their interface.

In order to study the response of the material structure subject to general loading conditions in 3D several models explicitly representing the geometrical distribution of fibers have been introduced using the finite element method (Radtke *et al.*, 2010) or lattice models (Bolander and Saito, 1997; Leite *et al.*, 2004). For purely tensile loading, models applying simplifying assumptions about the geometrical layout of the composite with respect to the tensile loding direction have been formulated with the goal to describe the tensile strain-hardening behavior. These models reflect the fragmentation process of composites starting from an elastic range, over a gradual evolution of matrix cracks with reinforcement strain localization up to a saturated crack density and/or ultimate failure of the weakest crack bridge.

The strain-hardening response of composites with elastic-brittle matrix and elastic reinforcement or similarly elastic-brittle reinforcement and elastic matrix can be described in closed form. In their classical work

5th International Conference on Reliable Engineering Computing (REC 2012)
Edited by M. Vořechovský, V. Sadílek, S. Seitl, V. Veselý, R. L. Muhanna and R. L. Mullen

ISBN 978-80-214-4507-9. Published by Ing. Vladislav Pokorný − LITERA

Table I. State of the art overview

scheme	transverse	longitudinal	bond law	math	ref.
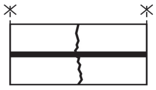	assumed homogeneous	periodic CS, const. length	constant	1D, analytical	(Aveston *et al.*, 1971; Aveston and Kelly, 1973)
	assumed homogeneous	exact CS length distribution	constant	1D, analytical	(Curtin, 1992; Ahn and Curtin, 1996)
	averaged micromechanical	simplified	arbitrary analytical	1D, analytical	(Li *et al.*, 1991; Chudoba *et al.*, 2006a)
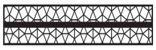	partly homogeneous	explicit cracks	arbitrary	1D (2D), numerical	(Konrad and Chudoba, 2009; Azzam and Richter, 2011)
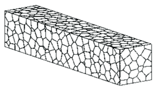	explicit micromechanical	explicit cracks	arbitrary	2D, 3D, numerical	(Bolander and Saito, 1997; Radtke *et al.*, 2010)

Aveston, Cooper and Kelly (Aveston *et al.*, 1971) formulated the explicit relation between stress and strain of the composites with constant matrix strength under the assumption of aligned continuous reinforcement with an ideally plastic bond to the matrix. Later, they extended the model for elastic-plastic bond and included the effect of random fiber orientation by correspondingly reducing the number of bridging fibers compared to the aligned mode (Aveston and Kelly, 1973). An energy release rate approach taking into account the elastic stretching of matrix and fibers, matrix cracks propagation and fiber debonding has been presented by (Budiansky *et al.*, 1986).

(Cho *et al.*, 1992) studied ceramic composites with aligned fibers and provided analytical formulas for the composite stress-strain diagram assuming elastic material properties and a more sophisticated bond law. Using the stress criterion for debonding, the formulation of Cho et al. delivers a set of closed form solutions describing the composite behavior and crack spacing distributions for three different ratios of matrix and debonding strength. Moreover, a numerical study was performed for random matrix strength following the two parameter Weibull distribution furnishing stress-strain diagrams and crack spacing distribution. A remarkable method for arriving at the exact crack spacing distribution was developed by (Curtin, 1991) for a single filament embedded in a large failure strain matrix with randomized filament strength and constant frictional bond. The results show good agreement with an extensive Monte Carlo simulation performed earlier by (Netravali *et al.*, 1989; Henstenburg and Phoenix, 1989).

Curtin later applied his theory to composites with multiple matrix cracks (Curtin, 1992) and found a connection between the matrix flaw distribution and the crack spacing of a composite loaded in tension. Since the initial matrix flaws have to propagate through the cross-section while consuming energy a lower threshold is introduced for the stress-at-first-crack distribution. Having fitted two independent parameters from a composite tensile test, this model is able to predict the composite behavior and estimate the frictional bond. Another estimation of the bond stress based on experiments was performed earlier by (Marshall and Evans, 1985) offering three different methods for this purpose. An inherently statistical evaluation of the

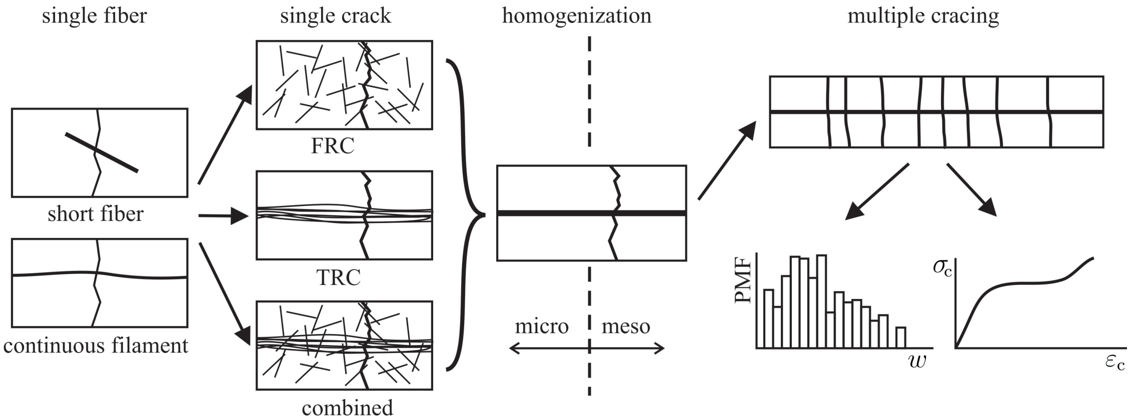

Figure 1. Scheme of the proposed model

stress-strain relationship and hysteretic behavior was performed by (Ahn and Curtin, 1996) and further simplified to closed forms by (Curtin *et al.*, 1998).

For composites with interface that can be described by one or a few bond parameters, e.g. for concrete reinforced with steel rebars, the aforementioned models can provide a realistic prediction. However, composites consisting of a large number of short or continuous fibers exhibit irregularities of the material structure (e.g. due random orientation of the fibers or due to an incomplete penetration of yarns by the matrix). The resulting variations in the stiffness and bond properties lead to a highly inhomogeneous microscopic bond stress fields. Such a field cannot be uniquely captured by a constant shear stress within the frictional bond model. This fact makes a more detailed resolution of the local stress and strain fields in the debonding zones inevitable. Models resolving the local fields in the vicinity in the crack bridge have been constructed using statistical averaging techniques (Li *et al.*, 1991; Chudoba *et al.*, 2006a; Kabele, 2003). With a higher computational effort, also finite element method has been used for local representation of the heterogeneous matrix-reinforcement bond structure (Konrad and Chudoba, 2009; Azzam and Richter, 2011; Nour *et al.*, 2011).

Table I summarizes the mentioned modeling approaches with a schematic picture of the assumed material representation. The models are classified according to the level of material resolution distinguished in transverse and longitudinal directions, kind of crack representation, applied bond law and dimensionality of the underlying mathematical formulation. In this paper a refined model for the simulation of strain-hardening response of a composite with heterogeneous structure of reinforcement is formulated. The effective stress –

Figure 2. TRC specimen reinforced with carbon fabrics after tensile test: localized failure crack (left), crack pattern (right)

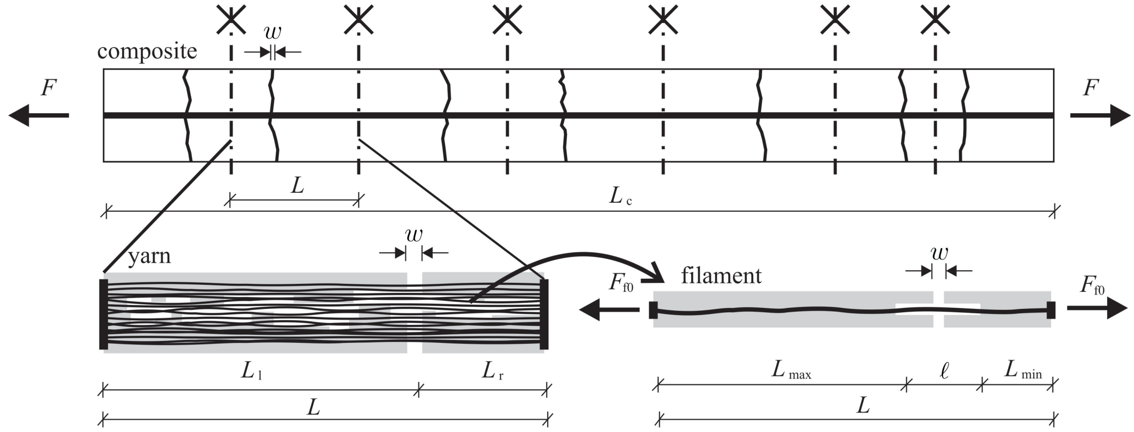

Figure 3. Application of the proposed model to textile reinforced concrete (from the top): homogenized composite model; statistical crack bridge model, microfilament double sided pullout model

strain relation is obtained using a multiscale homogenization procedure with separate integration loops at the micro- and mesoscale. At the microscale, the random structure of the reinforcement is reflected in the model of a representative crack bridge. At the mescoscale, the homogenization is performed over a representative series of emerging cracks sequentially introduced at positions where the matrix tensile stress reaches the level of the matrix strength.

The model components realizing the described homogenization procedure at the micro and mesoscales are depicted in Fig. 1. The hierarchical structure of the model opens up the possibility to include formulations of the crack bridge behavior for various types of reinforcement structure (e.g. short fibers, multifilament yarns or steel rebars) and their combinations. Let us also note, that the present modeling framework does not impose any limitations on the type of the bond law governing the interaction between fibers and matrix.

In order to make the explanation of the implementation of the model illustrative the formulation is provided for textile reinforced concrete consisting of a fine grained, brittle cementitious matrix reinforced by continuous multifilament yarns, such as AR-glass, carbon or aramid rovings (Fig. 2). The smallest scale considered deals with a single filament that bridges a matrix crack. The formulation of a single filament bridging a crack is provided in Sec. 2. A large number of such filaments form the reinforcing yarn which is assumed to be a multiple of the average filament response (Sec. 3). The evaluation of the homogenized strain field within a specimen with multiple cracks at a given level of stress is provided in Sec. 4. Results of computational examples showing some micromechanical dependencies on the global composite response are presented in Sec. 5 and concluding remarks summarize the capabilities and limitations of the model in Sec. 6.

2. Filament crack bridge model

At this level a single filament from a multifilament yarn embedded in matrix is observed and shall be represented by a parametric micromechanical model. For efficiency reasons, we assume symmetry at the half distance between adjacent cracks so that the filament is modeled only between two such symmetry points crossing a single crack and its boundary conditions are fixed (Fig. 3). As the loading is increased, the crack width grows, both matrix and filament are stretched and debonding takes place at the filament-matrix interface. Filaments are assumed to have constant geometrical and physical properties over the length. However, the properties vary for individual filaments because they can, in general, have different physical, geometrical and bond properties. These assumptions together with linear elastic behavior of the matrix result in the following formulation for the filament response in terms of bridging force vs. crack width relationship:

$$F_{\mathrm{f0}} = F_{\mathrm{f0}}(w, A_{\mathrm{m}}, E_{\mathrm{m}}, L_{\mathrm{l}}, L_{\mathrm{r}}, \boldsymbol{\theta}_{\mathrm{f}}), \quad \boldsymbol{\theta}_{\mathrm{f}} = \{A_{\mathrm{f}}, E_{\mathrm{f}}, \tau, \ell, \theta, \xi, p\} \tag{1}$$

where the control variable w is the crack width, $A_{\mathrm{m/f}}$ and $E_{\mathrm{m/f}}$ the matrix/filament cross-sectional area and modulus of elasticity, respectively, $L_{\mathrm{l/r}}$ are distances from the crack to the boundaries at the left/right hand side, τ stands for the friction acting at the matrix-filament interface, ℓ denotes the bond free length of the filament, θ is the filament waviness in terms of additional strain (delayed activation), ξ is the filament breaking strain and p is the filament perimeter. Variables summarized in $\boldsymbol{\theta}_{\mathrm{f}}$ are the filament properties which are later in Sec. 3 eventually considered as random. For simplicity only the control variables w, x will be explicitly indicated further in the text.

Three stages (Fig. 4) of the filament crack bridge response have to be distinguished in the explicit notation:

(A) First, debonding (the bond law assumed here is a frictional resistance with constant magnitude τ) takes place at both sides of the crack and propagates towards the (fixed) boundaries

$$F_{\mathrm{f0(A)}}(w) = \begin{cases} \dfrac{1}{2\eta^2}\left(\sqrt{c_{\mathrm{A}}^2 + 4w_\theta K_{\mathrm{f}}\eta^2 T} - c_{\mathrm{A}}\right), & w_\theta \geq 0 \\ 0, & w_\theta < 0 \end{cases} \tag{2}$$

$$c_{\mathrm{A}} = LT - \eta(L_{\mathrm{min}} + L_{\mathrm{max}})T, \tag{3}$$

ℓ_θ and w_θ include the effect of the filament waviness in the following way: $\ell_\theta = \ell(1+\theta); w_\theta = w - \theta\ell$. $T = \tau p$ denotes the shear flow per unit length of a filament with the perimeter p, $K_{\mathrm{f/m}}$ is the filament/matrix tensile stiffness defined as $A_{\mathrm{f/m}}E_{\mathrm{f/m}}$ and η stands for the matrix/composite stiffness ratio $K_{\mathrm{m}}/(K_{\mathrm{f}} + K_{\mathrm{m}})$. $L_{\mathrm{min/max}}$ is the shorter/longer bonded length at the left or right hand side from the crack and is defined as $\min/\max\{L_{\mathrm{l}} - \ell/2, L_{\mathrm{r}} - \ell/2\}$ and L is the total filament length in the crack bridge (see Fig. 3).

(B) As soon as the debonding reaches the closer boundary, i.e. the bond is activated along the whole primarily bonded length L_{min} (Fig. 3) the model formally changes from a crack bridge to a pullout with free fiber length ℓ_{e} equal to $2L_{\mathrm{min}} + \ell$, bonded length L_{b} defined as $L_{\mathrm{max}} - L_{\mathrm{min}}$ and a force offset P_{A} accumulated in stage A due to the frictional bond along the debonded interface:

$$F_{\mathrm{f0(B)}}(w) = \frac{1}{\eta^2}\left(\sqrt{c_{\mathrm{B}}^2 + 2(w_\theta - w_{\theta,\mathrm{A}})K_{\mathrm{f}}\eta^2 T} - c_{\mathrm{B}}\right) + P_{\mathrm{A}} \tag{4}$$

$$c_{\mathrm{B}} = LT - \eta(L_{\mathrm{max}} - L_{\mathrm{min}})T \tag{5}$$

with $w_{\theta,\mathrm{A}}/P_{\mathrm{A}}$ the crack width/force at the transition between stage A and B.

(C) After the filament has been fully debonded along the whole length L, the model responses linearly-elastic to further loading with tensile stiffness K_f:

$$F_{\mathrm{f0(C)}}(w) = \frac{K_\mathrm{f}(w_\theta - w_{\theta,\mathrm{B}})}{L} + P_\mathrm{B}. \tag{6}$$

where $w_{\theta,\mathrm{B}}/P_\mathrm{B}$ in analogy to Eq. (4) stand for the crack width/force at the transition between stage B and C.

Putting Eqns. (2, 4, 6) together yields the formula for the bridging force F_{f0}:

$$F_{\mathrm{f0}}(w) = \begin{cases} P_{\mathrm{f0(A)}} & : 0 \leq F_{\mathrm{f0}} < P_\mathrm{A} \\ P_{\mathrm{f0(B)}} & : P_\mathrm{A} \leq F_{\mathrm{f0}} < P_\mathrm{B} \\ P_{\mathrm{f0(C)}} & : P_\mathrm{B} \leq F_{\mathrm{f0}} \end{cases} \tag{7}$$

Filament can break anytime during the loading which causes an immediate drop of the bridging force to zero. The remaining force carried by a broken filament being pulled out of the matrix is assumed to have minor contribution compared to intact filaments and is therefore neglected. This can be written using the Heaviside step function $H(x)$ defined as:

$$H(x) = \begin{cases} 0 & : x < 0 \\ 1 & : x > 0 \end{cases} \tag{8}$$

resulting in:

$$F_{\mathrm{f0}}(w) = F_{\mathrm{f0}} \cdot H(F_{\mathrm{f0}} - A_\mathrm{f} E_\mathrm{f} \xi) \tag{9}$$

Eqn. (7) delivers a base for the evaluation of strains in the filament $\varepsilon_\mathrm{f}(x)$ and matrix along the longitudinal axis x (Fig. 4). Highest values of filament strain occur at the crack position and with growing distance from the crack linearly descend with slope equal to the shear flow per length value T provided that the filament has a bond to the matrix. If there is a part of the filament with no contact to the matrix, the strain is constant along the region (see lower diagrams in Fig. 4). However, there is a lower bound $\varepsilon_{\mathrm{ff}}$ for the filament strain which equals the far field strain of the compact composite where no debonding takes place:

$$\varepsilon_{\mathrm{ff}}(w) = \frac{F_{\mathrm{f0}}}{K_\mathrm{m} + K_\mathrm{f}}. \tag{10}$$

The strain along a filament can be expressed as:

$$\varepsilon_\mathrm{f}(w, x) = \begin{cases} F_{\mathrm{f0}}/K_\mathrm{f} & : \text{free length } \ell_\mathrm{e} \\ \left[F_{\mathrm{f0}} - T\left(|x| - \ell_\theta/2\right)\right]/K_\mathrm{f} & : \text{debonded part } a \\ \varepsilon_{\mathrm{ff}} & : \text{bonded part } L_{\mathrm{PO}} - a \end{cases} \tag{11}$$

where the variable x is the position at the longitudinal axis with origin at the crack.

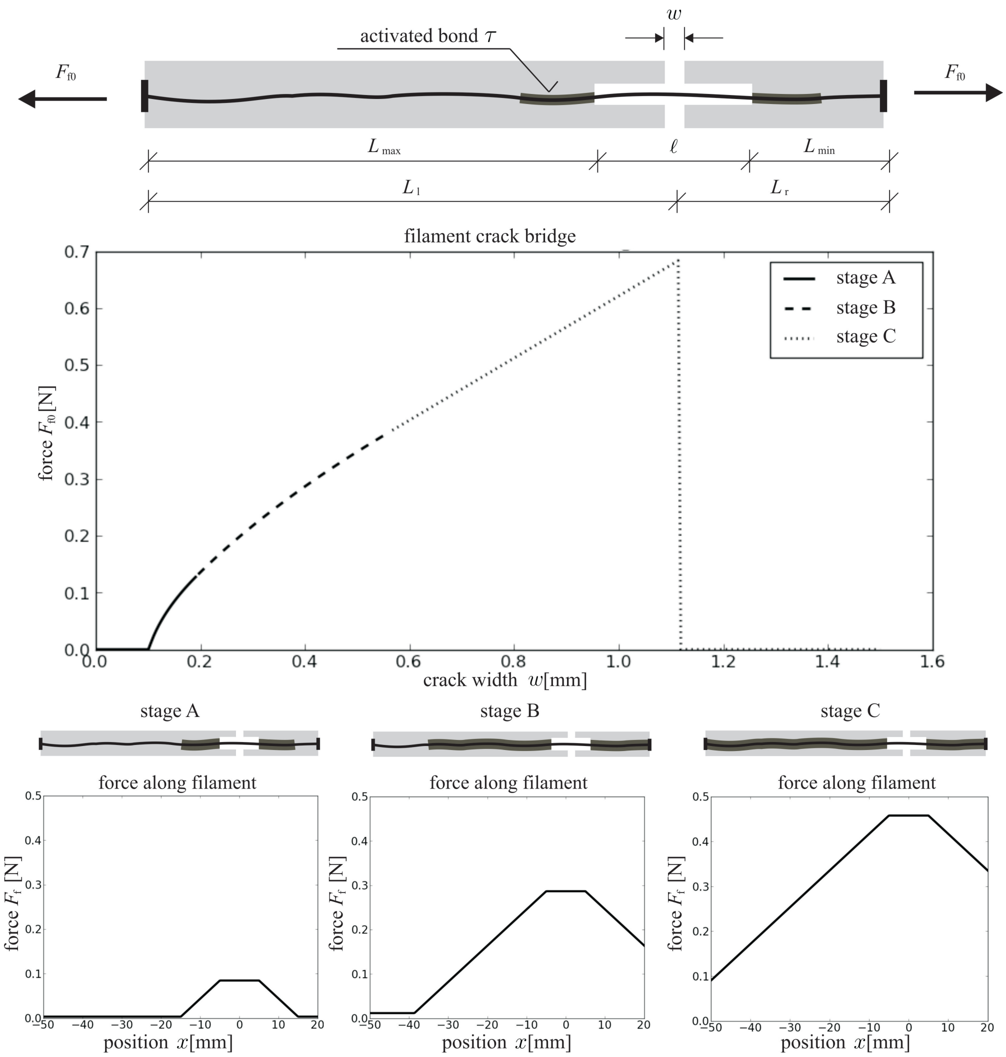

Figure 4. Filament crack bridge - force vs crack width with 3 distinguished phases (upper diagram); force in filament along the longitudinal axis for debonding stages A, B and C (lower diagrams). Parameters: $A_m = 29.4 \cdot 10^{-3}$ [mm^2], $E_m = 30 \cdot 10^3$ [MPa], $L_l = 50$ [mm], $L_r = 20$ [mm], $A_f = 5.31 \cdot 10^{-4}$ [mm^2], $E_f = 72 \cdot 10^3$ [MPa], $\tau = 0.1$ [N/mm^2], $\ell = 10$ [mm], $\theta = 0.01$ [-], $\xi = 0.0179$ [-], $p = 85.0 \cdot 10^{-3}$ [mm]. The three profiles are depicted for crack widths $w = 0.15$, 0.4 and 0.7 mm (from left to right).

3. Statistical crack bridge model

Sec. 2 creates a basis for the yarn crack bridge model. Since yarns consist of several hundreds or thousands of filaments, it would be very inefficient to simulate every single filament and sum their contributions. Therefore, the yarn is assumed to be represented by the average filament multiplied by the total number of filaments:

$$F_{y0}(w) = N_f \cdot \mu_{f0} = N_f \cdot E\left[F_{f0}\right] \tag{12}$$

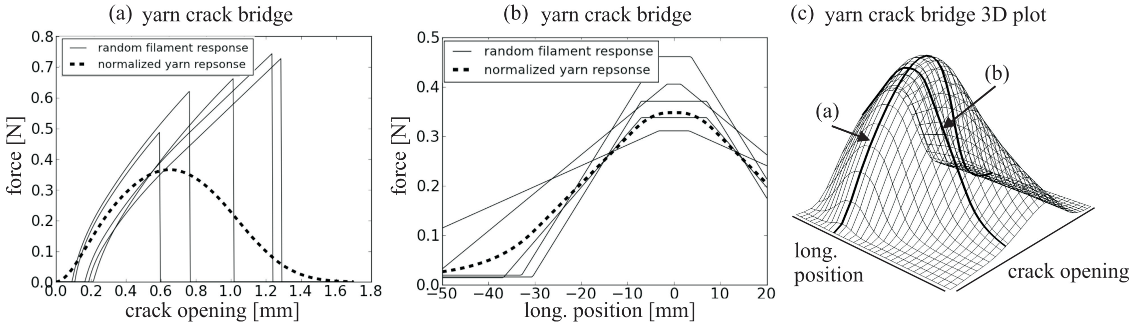

Figure 5. Yarn crack bridge - normalized yarn force F_{y0}/N_f vs crack opening and 5 random filament realizations (a); normalized yarn force F_y/N_f along longitudinal axis and 5 random filament realizations (b); 3D plot of the diagrams (c). Parameters for the yarn response: $A_m = 50.0$ [mm^2], $E_m = 30 \cdot 10^3$ [MPa], $L_l = 50$ [mm], $L_r = 20$ [mm], $A_f = 5.31 \cdot 10^{-4}$ [mm^2], $E_f = 72 \cdot 10^3$ [MPa], $\tau = \mathrm{uniform\,distribution\,(min} = 0.05,\ \mathrm{max} = 0.20)$ [N/mm^2], $\ell = \mathrm{uniform\,distribution\,(min} = 2.0,\ \mathrm{max} = 17.0)$ [mm], $\theta = 0.01$ [-], $\xi = \mathrm{Weibull\,distribution\,(shape} = 5.0,\ \mathrm{scale} = 0.0179$ [-], $p = 85.0 \cdot 10^{-3}$ [mm], $N_f = 1700$ [-]. The profiles in (b) are depicted for the crack width $w = 0.5$ mm.

for the force vs crack width and

$$F_y(w, x) = N_f \cdot \mu_f = N_f \cdot E[F_f] \tag{13}$$

for the force along the yarn. The average or expected value of the filament crack bridge response μ_{f0} and μ_f multiplied by the total number of filaments N_f can be alternatively written as follows:

$$F_{y0}(w) = E[F_{f0}(A_f = A_y, p = N_f \cdot p)] \tag{14}$$

and

$$F_y(w, x) = E[F_f(A_f = A_y, p = N_f \cdot p)] \tag{15}$$

respectively. This approach was used earlier e.g. for modeling fiber bundles with random fiber properties in (Phoenix, 1979; Phoenix and Taylor, 1973; Chudoba *et al.*, 2006b) and in the early works (Daniels, 1945; Coleman, 1958). Assumed that the filaments are statistically and mechanically independent it delivers an asymptotic result (for an infinite number of filaments) which is in this case justified by the large number of filaments forming a yarn. The average filament response (Fig. 5) is evaluated as stated in the cited literature in the following way:

$$\mu_{f0}(w) = \int_{\boldsymbol{\theta}_f} F_{f0} \cdot f(\boldsymbol{\theta}_f)\, \mathrm{d}\boldsymbol{\theta}_f \tag{16}$$

for the force resisting the crack opening and

$$\mu_f(w, x) = \int_{\boldsymbol{\theta}_f} F_f \cdot f(\boldsymbol{\theta}_f)\, \mathrm{d}\boldsymbol{\theta}_f \tag{17}$$

for the force along the composite longitudinal axis, with $f(\boldsymbol{\theta}_f)$ denoting the joint probability density function (PDF) of the random variables from the vector $\boldsymbol{\theta}_f$. The average filament responses μ_{f0} and μ_f are depicted in Fig. 5.

4. Composite model with stochastic cracking

With equations defined in Sec. 3 all tools needed for describing the stress state in the composite around a crack are provided. However, composite materials are designed to fail only after multiple transverse cracks have formed. To model this behavior, two additional variables have to be introduced: the load level F for new cracks to form and positions x_c of the cracks. F and x_c are revealed by satisfying the following condition:

$$\sigma_\mathrm{m}(F, x) \geq \sigma_\mathrm{mu}(x) \tag{18}$$

where σ_mu is a static autocorrelated random field (Vorechovsky, 2008). We define the local matrix strength as having the distribution of minimum extremes according to Weibull

$$W(\sigma_\mathrm{mu}) = 1 - \exp\left(-\left\langle \frac{\sigma_\mathrm{mu}}{\sigma_0} \right\rangle^m\right) \tag{19}$$

with m and σ_0 standing for the shape and scale parameter, respectively, and being cross correlated by the following definition

$$R(\mathrm{d}x, l_\rho) = \exp\left(-\frac{\mathrm{d}x}{l_\rho}\right)^2 \tag{20}$$

where l_ρ is the autocorrelation length and $\mathrm{d}x$ the distance between two points in the random field. The random field mimics the natural fluctuations of the local strength of reinforced matrix and automatically ensures the random distribution of the first cracks along the specimen (Fig. 6). A realization of this random field σ_mu is at a given load compared with the stress state in matrix σ_m and cracks are formed at the load level F and position x_c where the two functions first overlap if F is monotonically increased (Fig. 7).

4.1. Computation of σ_m

At small tensile loads at the beginning of the loading process, the strains in both matrix and reinforcement are assumed to be constant along the longitudinal axis x and described by:

$$\varepsilon_\mathrm{ff}(F) = \frac{F}{K_\mathrm{f} + K_\mathrm{m}} \tag{21}$$

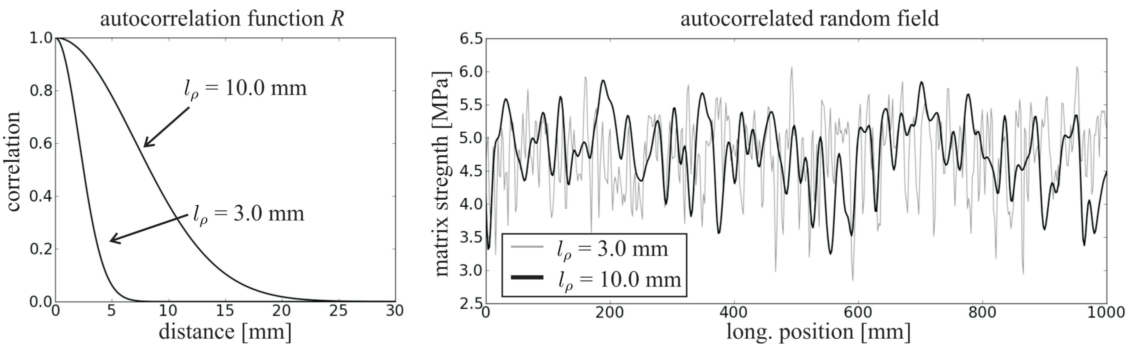

Figure 6. Autocorrelation function for $l_\rho = 3.0$ and 10.0 mm (left); corresponding realizations of a Weibull (shape = 10.0, scale = 5.0, location = 0.0) random field (right)

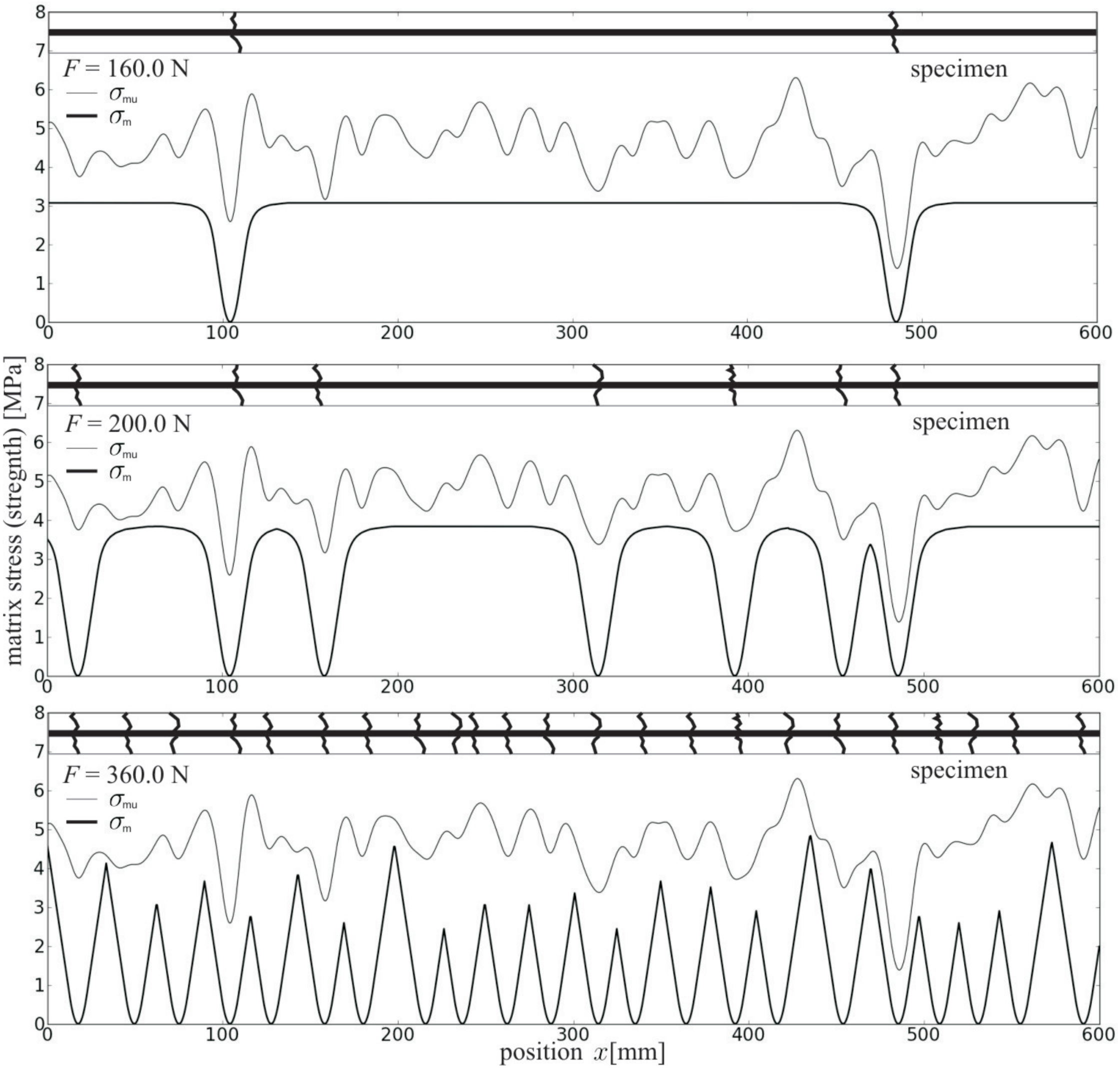

Figure 7. Matrix stress profiles at various loading stages

As soon as the tensile strength of the matrix is reached at some place, a matrix crack forms, the forces are redistributed and the reinforcement strain localizes at the position of the matrix crack (Fig. 7). Analogically, strain in the matrix drops to zero and is built up with growing distance from the crack. Cohesive forces between the newly created matrix surfaces are ignored here. The current matrix stress, given the yarn force by Eq. (15), is evaluated as:

$$\sigma_{\mathrm{m}}(F,x) = \frac{F - F_{\mathrm{y}}}{A_{\mathrm{m}}} \tag{22}$$

where the half distances to the neighboring cracks L_{l} and L_{r}, respectively, have to be taken into account and substituted into F_{y} in Eq. (15). Since F_{y} is controlled by crack opening, the value of crack opening corresponding to the applied load F has to be evaluated first. This can be done by inverting Eq. (16) so that $\mu_{\mathrm{f0}}(w)$ becomes $w(\mu_{\mathrm{f0}})$ where μ_{f0} is substituted by the applied load F. In this way, F_{y} in Eq. (15) is redefined as a function of F.

4.2. Average composite strain

The strain profile along the yarn has to be evaluated at every load step as it is qualitatively and quantitatively affected by both the load level and the crack positions. The overall (average) strain of the composite loaded in tension is evaluated by integrating the yarn strain, which is the parallel coupling of yarn strain profiles within the individual crack bridges $\varepsilon_{\mathrm{y}} = F_{\mathrm{y}}/(E_{\mathrm{f}} A_{\mathrm{y}})$, along the whole specimen - delivering the total displacement - and dividing it by the composite specimen length L_{c}:

$$\varepsilon_{\mathrm{c}}(F) = \frac{1}{L_{\mathrm{c}}} \int_0^{L_{\mathrm{c}}} \varepsilon_{\mathrm{y}}(F, x) \mathrm{d}x \tag{23}$$

5. Computational examples

To demonstrate the influence of randomized parameters we observe the composite stress – strain diagram Eq. (23) and the crack width distribution. Parameters shall be varied 'one at the time' to point out their particular contribution to the global response.

5.1. Random matrix strength

Defining the matrix strength by a constant value results in a horizontal line in the stress – strain diagram (ACK (Aveston *et al.*, 1971)) at the composite stress level, which corresponds to the ultimate matrix stress. If the local matrix strength fluctuates around this value, cracks develop at earlier load stages (Fig. 8). In fact, the load at first crack is distributed as the minimum extreme value of the random matrix strength. Furthermore, the composite response is also affected by the predominant correlation of the matrix strength. If the fine grains are the main source of strength correlation, the autocorrelation length l_ρ is rather small. In contrary, a nearly homogeneous matrix with strength fluctuations caused predominantly by outer sources (e.g. casting process, geometrical inaccuracies) can be expected to have a large l_ρ. A case in between these extremes is e.g. the cross-section strength reduction caused by fine shrinkage cracks. Here, the l_ρ of the matrix strength is in the order of a few millimeters. In Fig. 9, the filament and bond parameters are fixed and l_ρ of the matrix strength is varied to represent the three cases mentioned. In the range of approx. $1.0 < \delta_0/l_\rho < 10.0$, where

$$\delta_0 = \frac{(K_{\mathrm{m}} + K_{\mathrm{f}})\sigma_0}{E_{\mathrm{m}} T} \tag{24}$$

is the shielded length and σ_0 is the scale parameter of the matrix strength distribution, the autocorrelation length l_ρ has a significant influence on the degree of tension stiffening - the difference in strains of a composite saturated with crack and of the reinforcement only. It is proportional to the stress remaining in the matrix in the saturated state (gray shaded area in Fig. 9) which on the other hand is proportional to the distance of minimums of the matrix strength For high δ_0/l_ρ ratios, the minimums of matrix strength along

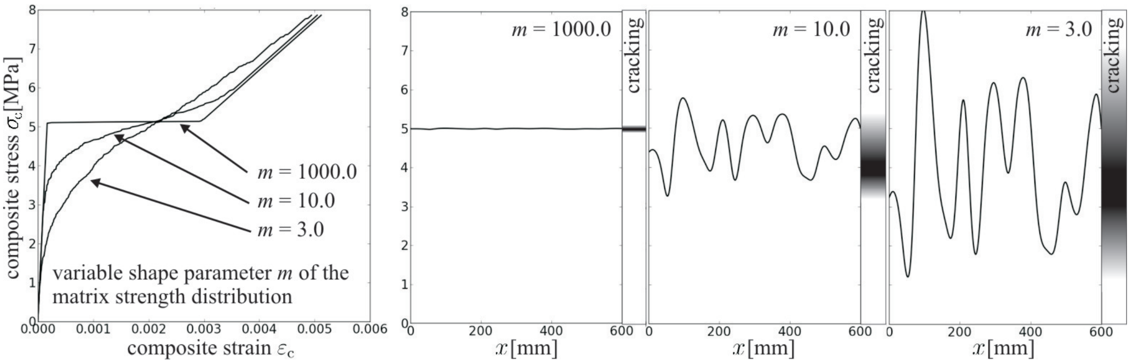

Figure 8. Variable shape parameter m of the matrix strength distribution. Stress – strain diagrams (left), matrix strength along x for variable m (right). Parameters: $A_\mathrm{m} = 50.0$ [mm^2], $E_\mathrm{m} = 30 \cdot 10^3$ [MPa], $L_\mathrm{c} = 3000$ [mm], $A_\mathrm{f} = 5.31 \cdot 10^{-4}$ [mm^2], $E_\mathrm{f} = 72 \cdot 10^3$ [MPa], $\tau = 0.1$ [N/mm^2], $\ell = 0.0$ [mm], $\theta = 0.0$ [-], $\xi = \infty$ [-], $p = 85.0 \cdot 10^{-3}$ [mm], $N_\mathrm{f} = 1700$ [-], σ_mu = autocorrelated field with Weibull distribution (shape = 3.0, 10.0, 1000.0, scale = 5.0, l_ρ = 30.0 [mm])

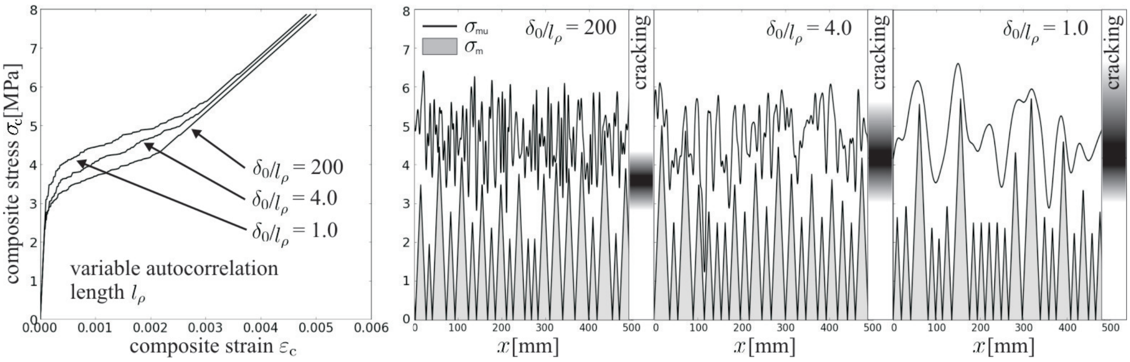

Figure 9. Variable autocorrelation length l_ρ of the matrix strength distribution. Stress – strain diagrams (left), matrix strength σ_mu along x for variable l_ρ and matrix stress $\sigma_\mathrm{m}(x)$ in saturated state (right). Parameters: $A_\mathrm{m} = 50.0$ [mm^2], $E_\mathrm{m} = 30 \cdot 10^3$ [MPa], $L_\mathrm{c} = 3000$ [mm], $A_\mathrm{f} = 5.31 \cdot 10^{-4}$ [mm^2], $E_\mathrm{f} = 72 \cdot 10^3$ [MPa], $\tau = 0.1$ [N/mm^2], $\ell = 0.0$ [mm], $\theta = 0.0$ [-], $\xi = \infty$ [-], $p = 85.0 \cdot 10^{-3}$ [mm], $N_\mathrm{f} = 1700$ [-], σ_mu = autocorrelated field with Weibull distribution (shape = 7.0, scale = 5.0, δ_0/l_ρ = 200.0, 4.0, 1.0)

x are close, so that the matrix cracking takes place mainly at lower stresses and the composite achieves the saturated state at relatively low loading stages. The crack spacing is dense and consequently there is not much stress remaining in the matrix in the saturated state. Low δ_0/l_ρ ratios result in a wider load range of matrix cracking, the saturated state is reached at higher load stages, the crack spacing is larger and the amount of stress stored in the matrix is higher.

The two examples demonstrate the feasibility of the implementation and its capability to reflect the effect of microstructural parameters on the strain-hardening response of the composite. Systematic parametric studies are currently being elaborated and will be presented in the following papers and during the conference presentation.

6. Concluding remarks

The paper describes a multiscale approach for modeling of the fragmentation process of composites with heterogeneous reinforcement. Components of the model were presented separately according to their respective scales. We have presented some results in Sec. 5, which reflect the sensitivity of the global composite behavior on the matrix strength distribution.

We remark that the matrix strength is represented by a single realization of a random field. Consequently, the results are single realizations of a function of random variables. However, the single realizations can be considered as fairly close to the expected values as the length of the modeled specimen $L_{\rm c}$ gets large compared to the autocorrelation length and therefore the variability, according to the central limit theorem, diminishes with the rate $\approx l_\rho / L_{\rm c}$. We kept this principle in mind when evaluating the presented results.

Summary of assumptions imposed in the model:

- loading results in uniaxial stress in the composite
- cracks are planar and perpendicular to the loading direction
- crack opening is uniform across the composite cross section

7. Acknowledgements

The work has been supported by the German Science Foundation under project number CH276/2-1 and SFB532/T05. Additionally, the work of the first and third author has been supported by the Czech Science Foundation under reg. no. P105/10/J028 and GD 103/09/H085. This support is gratefully acknowledged.

References

B. K. Ahn and W. A. Curtin. Strain and hysteresis by stochastic matrix cracking in ceramic matrix composites. *Journal of the Mechanics and Physics of Solids*, 45 (2):177 – 209, 1996.

J. Aveston and A. Kelly. Theory of multiple fracture of fibrous composites. *J. Mat. Sci. 8*, pages 411–461, 1973.

J. Aveston, G. Cooper, and A. Kelly. Single and multiple fracture, the properties of fibre composites. *Proc. Conf. National Physical Laboratories, IPC Science and Technology Press Ltd. London*, pages 15–24, 1971.

A. Azzam and M. Richter. Investigation of stress transfer behavior in textile reinforced concrete with application to reinforcement overlapping and development lengths. In Ortlepp R. Curbach, M., editor, *6th Colloquium on Textile Reinforced Structures (CTRS6)*, pages 103–116, 2011.

J.E. Bolander and S. Saito. Discrete modeling of short-fiber reinforcement in cementitious composites. *Advanced Cement Based Materials*, 6:76–86, 1997.

B. Budiansky, J.W. Hutchinson, and A.G. Evans. Matrix fracture in fiber-reinforced ceramics. *J. Mech. Phys. Solids*, 34(2):167–189, 1986.

Ch. Cho, J.W. Holmes, and J.R. Barber. Distribution of matrix cracks in a uniaxial ceramic composite. *J. Am. Ceram. Soc.*, 2(75):316–324, 1992.

R. Chudoba, M. Vorechovsky, J. Jerabek, and M. Konrad. Trc-specimens modeled as a chain of cracks. In *ECF16 16th European Conf. of Fracture*, 2006.

R. Chudoba, M. Vorechovsky, and M. Konrad. Stochastic modeling of multifilament yarns. I. Random properties within the cross-section and size effect. *International Journal of Solids and Structures*, 43(3-4):413–434, 2006.

B. D. Coleman. On the strength of classical fibres and fibre bundles. *Journal of Mechanics and Physics of Solids*, 7:60–70, 1958.

W.A. Curtin, B.K. Ahn, and N. Takeda. Modeling brittle and tough stress-strain behavior in unidirectional ceramic matrix composites. *Acta materialia*, 46(10):3409–3420, 1998.

W.A. Curtin. Exact theory of fiber fragmentation in a single-filament composite. *Journal of Materials Science*, 26:5239–5253, 1991.

W.A. Curtin. Multiple matrix cracking in brittle matrix composite. *Acta metall. mater.*, 41(5):1369–1377, 1992.

H. E. Daniels. The statistical theory of the strength of bundles of threads. i. *Proceedings of the Royal Society of London. Series A, Mathematical and Physical Sciences*, 183(995):405–435, 1945.

A.P. Fantilli, H. Mihashi, and P. Vallini. Multiple cracking and strain hardening in fiber reinforced concrete under uniaxial tension. *Cement and Concrete Research*, 39:1217–1229, 2009.

R.B. Henstenburg and S.L. Phoenix. Interfacial shear strength studies using the single-filament-composite test. part ii: A probability model and monte carlo simulation. *Polymer Composites*, 10(5):389–408, 1989.

P. Kabele. New developments in analytical modeling of mechanical behavior of ecc. *Journal of Advanced Concrete Technology*, 1(3):253–264, 2003.

M. Konrad and R. Chudoba. Tensile behavior of cementitious composite reinforced with epoxy impregnated multifilament yarns. *International Journal for Multiscale Engineering*, 7(2):115–133, 2009.

J.P.B. Leite, V. Slowik, and H. Mihashi. Computer simulation of fracture processes of concrete using mesolevel models of lattice structures. *Cement and Concrete Research*, 34:1025–1033, 2004.

V.C. Li and H.C. Wu. Conditions for pseudo strain-hardening in fiber reinforced brittle matrix composites. *Appl. Mech. Rev.*, 45(8):390–398, 1992.

V. C. Li, Y. Wang, and S. Backer. A micromechanical model of tension-softening and bridging toughening of short random fiber reinforced brittle matrix composites. *Journal of the Mechanics and Physics of Solids*, 39(5):607–625, 1991. fiber orientation considered by probabillity distribution function.

D.B. Marshall and A.G. Evans. Failure mechanisms in ceramic-fiber ceramic-matrix composites. *J. Am. Ceram. Soc.*, 68(5), 1985.

A.N. Netravali, R.B. Henstenburg, S.L. Phoenix, and P. Schwartz. Interfacial shear strength studies using the single-filament-composite test. i: Experiments on graphite fibers in epoxy. *Polymer Composites*, 10(4):226–241, 1989.

A. Nour, B. Massicotte, R. Montaignac, and J.P. Charron. Derivation of a crack opening deflection relationship for fibre reinforced concrete panels using a stochastic model: Application for predicting the flexural behaviour of round panels. *Cement and Concrete Research*, 41:964–974, 2011.

S.L. Phoenix and H.M. Taylor. The asymptotic strength distribution of a general fiber bundle. *Advances In Applied Probability*, 5:200 – 216, 1973.

S. L. Phoenix. Statistical theory for the strength of twisted fiber bundles with applications to yarns and cables. *Textile Research Journal*, 49:407–423, 1979.

F.K.F. Radtke, A. Simone, and L.J. Sluys. A computational model for failure analysis of fibre reinforced concrete with discrete treatment of fibres. *Engineering Fracture Mechanics*, 77:597–620, 2010.

M. Vorechovsky. Simulation of simply cross correlated random fields by series expansion methods. *Structural safety*, (30):337363, 2008.